PCCP

Cite this: *Phys. Chem. Chem. Phys.*, 2012, **14**, 7131–7136

www.rsc.org/pccp

PAPER

The combination of a polymer–carbon composite electrode with a high-absorptivity ruthenium dye achieves an efficient dye-sensitized solar cell based on a thiolate–disulfide redox couple†

Jing Zhang,[a] Huijin Long,[a] Sara G. Miralles,[b] Juan Bisquert,[b] Francisco Fabregat-Santiago*[b] and Min Zhang*[a]

Received 14th March 2012, Accepted 14th March 2012
DOI: 10.1039/c2cp40809k

To overcome the intrinsic shortcomings of the traditional iodide–triiodide redox couple and pursue a further performance improvement, intense efforts have been made to exploit alternative redox shuttles in dye-sensitized solar cells (DSCs). Herein, we report an energetic and kinetic view of DSCs when the iodine electrolyte is substituted with its thiolate counterpart and identify that a conventional platinum counter electrode presents low catalytic activity for the thiolate electrolyte, featuring a high charge transfer resistance found at the platinized fluorine-doped tin oxide (FTO). We employ conductive carbon black with several polymers to fabricate highly active composite catalysts for thiolate regeneration. The use of a highly active conductive carbon black and polymerized 3,4-ethylenedioxythiophene composition as a counter electrode combined with a high-absorptivity ruthenium dye C106 sensitized titania film has generated a DSC with an organic thiolated electrolyte, exhibiting an overall power conversion efficiency of 7.6% under AM1.5G full sunlight.

Introduction

As a potential substitute for the traditional fuel energy sources that are currently being exhausted, the dye-sensitized solar cell (DSC)[1] has attracted extensive interest in both academic and industrial fields. In a typical DSC, the iodide–triiodide redox shuttle is the most common choice, owing to an expeditious dye regeneration, a sluggish recombination between photoinjected electrons in titania and triiodide and a rapid mass transport of redox ions in a thin-layer sandwich device architecture.[2] However, the ordinary iodine electrolyte also presents some prominent constraints on the development of new photosensitizers, semiconductors and counter electrodes.[3] Recently, intense endeavors have been made to explore alternative redox couples to replace the iodine shuttle, such as metal complexes, halogens, pseudohalogens and some metal-free organic redox shuttles.[4] The thiolate–disulfide (T^-–T_2) organic redox couple (Fig. S1†) exploited by Grätzel *et al.* achieved the highest efficiency of 6.4% in iodine-free DSCs at that time.[4q] In comparison with the iodine cell, the thiolate counterpart exhibited lower open-circuit photovoltage (V_{oc}) and fill factor (FF). To further enhance the photovoltaic performance of this kind of cell, it is necessary to develop an in-depth understanding of energetics and kinetics of these two DSCs with different electrolytes.

It is found that the charge transfer resistance at the Pt/thiolate electrolyte interface is larger than that for the Pt/iodine case which explains the better FF attained with the iodine electrolyte. Because of the benign conduction, high specific surface area and low cost, the carbon materials have been applied as counter electrodes (CEs) in DSCs.[5] Carbon black is a good electrical conductor and shows high catalytic activity for the reduction of triiodide. An efficiency as high as 9.1% has been obtained for iodine-based DSCs with a carbon black counter electrode.[5e] However, the catalytic activity of carbon black for thiolate–disulfide is insufficient.

In this work, through a joint spectroscopic and electrical study on the energetics and kinetics of DSCs, we will take a close look at the origins of the redox couple influences on the photocurrent action spectra and current–voltage (j–V) curves of DSCs, by formulating two kinds of electrolytes characteristic of thiolate and iodine redox shuttles, respectively. On the basis of the aforementioned understanding, we will combine conductive carbon blacks (CCBs) with several polymers that have been proved to actively catalyze the reduction of triiodide to fabricate high active composite catalysts for thiolate regeneration. Integrating CCB and a polymerized 3,4-ethylenedioxythiophene (PEDOT) composition with a high-absorptivity ruthenium dye C106 (Fig. S1†) sensitized titania film and perfusing with an organic thiolate

[a] *Changchun Institute of Applied Chemistry, Chinese Academy of Science, Changchun 130022, China. E-mail: min.zhang@ciac.jl.cn; Fax: 86 431 852 629 53; Tel: 86 431 852 629 53*
[b] *Photovoltaic and Optoelectronic Devices Group, Physics Department, Universitat Jaume I, 12071 Castello, Spain. E-mail: fabresan@uji.es*

† Electronic supplementary information (ESI) available: Molecular structures, steady-state electronic absorption spectra, details of fitting of TAS and emission decay and electrochemical data. See DOI: 10.1039/c2cp40809k

electrolyte, our device achieved a 7.6% efficiency under AM1.5G full sunlight.

Results and discussion

We first measured the photocurrent action spectra of DSCs employing the thiolate and iodine electrolytes depicted in Fig. 1, in which the incident photon-to-collected electron conversion efficiencies (IPCEs) are plotted as a function of wavelength. As Fig. 1 presents, it can be seen that the electrolyte alteration from iodine to thiolate does not influence the IPCEs in the whole spectral range of 400–800 nm. Also note that although the iodine electrolyte exhibits higher absorption coefficients in the wavelength region of 400–450 nm (Fig. S2†), no noticeable difference in the IPCEs of the cells with these two electrolytes is observed in this spectral range, owing to the high-absorption-coefficient nature of our C106 dye.

Although comparable IPCE heights across the whole spectral response region with a maximum of ~86% were obtained with the thiolate and iodine electrolytes, it is still valuable to determine the net charge separation yields at the dye/titania/electrolyte interface and scrutinize the physical origins of non-ideal external quantum efficiencies. Transient absorption measurements were carried out to evaluate the kinetic competition between the recombination of photoinjected electrons and oxidized dye (D^+) and the interception of D^+ by the electron-donating species in electrolytes.[6] A monochromatic probe light at 782 nm was applied in transient kinetic measurements, where the excitation wavelength and fluence were carefully tuned to ensure that $\sim 1 \times 10^{14}$ photons cm^{-2} (~1.0 photon per particle) were absorbed by the dye-coated film, with an identical exciton distribution profile during every laser pulse. In the absence of electron-donating species in electrolytes, the absorption decay (trace **c** in Fig. 2A and B) can be attributed to the D^+ recombination with titania electrons, featuring a mean reaction time ($\langle\tau\rangle$) of 11 ± 0.4 ms calculated through a stretched exponential fitting (see Electronic Supplementary Information† for details). A further employment of the thiolate electrolyte remarkably accelerated the absorption decay (trace **a** in Fig. 2A) through electron donation from the thiolate to the oxidized dye molecules, producing a $\langle\tau\rangle$ of 14.5 ± 0.8 μs for the dye regeneration reaction. By comparison, the iodine electrolyte features a slightly faster dye regeneration rate with a 3.4 ± 0.4 μs mean reaction time (trace **b** in Fig. 2B). This displays a reverse dependence of the Gibbs free energy for dye regeneration, indicating that with respect to the routinely used iodine electrolyte, the sluggish dye regeneration of the thiolate counterpart should allow for a small elevation space of the ground-state redox potential in the future design of low energy gap dyes to harvest near-infrared solar photons. In spite of their dissimilar dye regeneration kinetics, however, the branch ratios of the dual-channel charge transfer kinetics were over 750 for both redox shuttles, exerting negligible influences on the IPCE maxima.

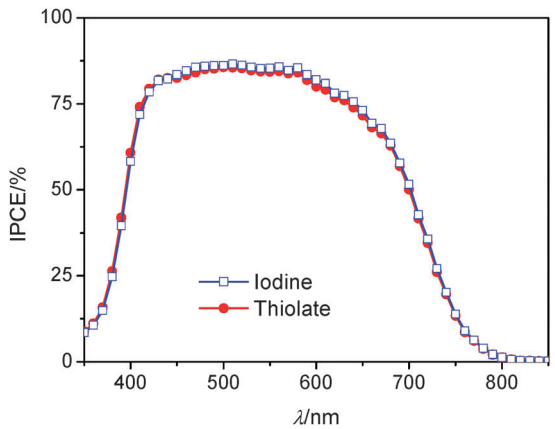

Fig. 1 Photocurrent action spectra of dye-sensitized solar cells with iodine and thiolate as redox species. The aperture area of the metal mask is 0.160 cm^2. An anti-reflection film was adhered to the testing cell during measurement.

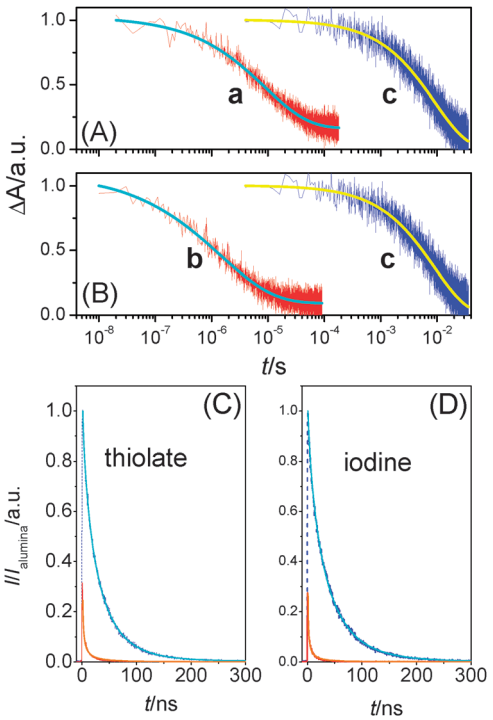

Fig. 2 (A) and (B) Kinetic traces in the (a) thiolate, (b) iodine and (c) inert electrolytes of a 12-μm-thick, C106-coated titania film. The smooth lines are stretched exponential fittings over the raw data obtained by averaging 800 laser shots. The excitation fluence is 44 μJ cm^{-2} at a wavelength of 665 nm. (C) and (D) Time-correlated emission decay traces of cells with titania or alumina film with an excitation wavelength of 488 nm. The detection wavelength was at the wavelength of the maximum emission intensity. The emission intensity (I) was corrected in terms of the film absorbance at 488 nm and further normalized with respect to the emission maximum of a dye-coated alumina film ($I_{max,alumina}$).

We resorted to the time-correlated single photon counting (TCSPC) technique to evaluate the exciton dissociation efficiency at the dye/titania interface.[7] A reference dummy cell was first constructed based on a C106-coated alumina film soaked in the thiolate or iodine electrolyte, which displays a strong photoluminescence (the blue lines in Fig. 2C and D) upon laser excitation at 488 nm. On account of the straddling dye/alumina junction, which is thermodynamically unfeasible for charge generation, we assign these emissions to the irradiative and non-irradiative deactivations of excited-state dye molecules. The time-correlated emission decay traces are well fitted with a

stretched exponential function (see the Electronic Supplementary Information† for details). The photoluminescence average lifetimes ($\langle\tau\rangle$) of the C106 dye molecules anchored on alumina in contact with the thiolate and iodine were calculated as 29.2 ± 0.16 and 34.2 ± 0.09 ns, respectively. Moreover, the emission average lifetimes on the titania film (the red lines in Fig. 2C and D) are notably reduced to 2.1 ± 0.09 and 1.6 ± 0.07 ns for the corresponding thiolate and iodine electrolytes. Hereby, we can derive the electron injection rate constants to be $(4.3 \pm 0.2) \times 10^8$ and $(6.0 \pm 0.3) \times 10^8$ s^{-1} for cells with thiolate and iodine electrolytes, respectively. Calculation with the photoluminescence average lifetimes on titania and on alumina affords comparable electron injection yields (η_{inj}) of $(93 \pm 0.3)\%$ and $(95 \pm 0.2)\%$ for the respective thiolate and iodine cells, which echoes the similar IPCE maxima mentioned above.

The solar-to-electricity conversion efficiencies were further evaluated by measuring the photocurrent density–voltage (j–V) characteristics (Fig. 3) at an irradiation of 100 mW cm^{-2} AM1.5G simulated sunlight and the photovoltaic parameters are collected in Table 1. The components of the previously optimized iodine based electrolyte were utilized in the iodine cell, which achieved the best power conversion efficiency of C106 under this film thickness. The short-circuit photocurrent density (j_{sc}), open-circuit photovoltage (V_{oc}) and fill factor (FF) of a typical cell with the iodine electrolyte are 17.1 mA cm^{-2}, 750 mV and 0.77, respectively, affording an overall power conversion efficiency (η) of 9.8%. The thiolate analogue exhibits a similar j_{sc}, in agreement with the preceding IPCE measurements, but it leads to a 90 mV decrease of V_{oc} from 750 to 660 mV in contrast to the iodine cell. This fact together with a decreased FF of 0.55 results in a lower η of 6.2%.

The relatively low V_{oc} for the thiolate cell may be explained by analyzing the energetics of the redox couple and conduction band position in TiO_2 (Fig. S3†) with an energy diagram, as plotted in Fig. 4a.[8] As observed in the figure, while the TiO_2 conduction band edge in thiolate is only 10 mV lower than in iodine, the redox potential for thiolate is 130 mV higher than for iodine. Consequently, the recombination resistance, and therefore the V_{oc}, is expected to be lower in the case of thiolate

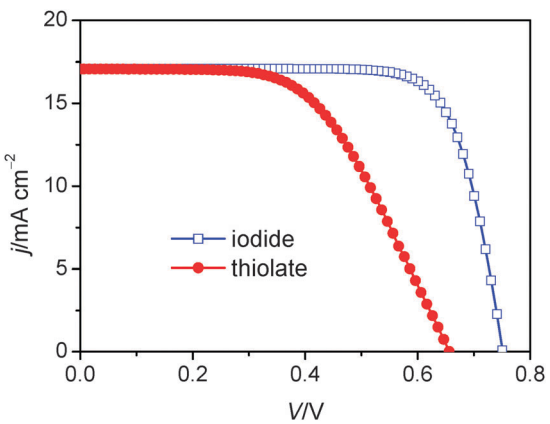

Fig. 3 j–V characteristic measured at an irradiation of 100 mW cm^{-2} AM1.5G sunlight for dye-sensitized solar cells with two different redox species. The counter electrode was a platinized FTO. The aperture area of the metal mask is 0.160 cm^2. An anti-reflection film was adhered to the testing cell during measurement.

Table 1 Photovoltaic data measured at an irradiation of 100 mW cm^{-2} AM1.5G sunlight[a]

Electrolyte	V_{oc}/mV	j_{sc}/mA cm^{-2}	FF	η (%)
Thiolate	660 ± 5	17.1 ± 0.02	0.55 ± 0.002	6.2 ± 0.05
Iodine	750 ± 5	17.1 ± 0.02	0.77 ± 0.001	9.8 ± 0.04

[a] The spectral distribution of our light resource simulates the AM1.5G solar emission (ASTM G173-03) with a mismatch of ~5%. The abbreviations in Table 1 stand for: open-circuit photovoltage V_{oc}; short-circuit photocurrent density j_{sc}; fill factor FF; total power conversion efficiency η, and charge transfer resistance from the counter electrode to the redox couple R_{CE}.

than for iodine. This is what was found in Fig. 4(b). Near V_{oc}, the differences in R_{rec} are 110 mV coincident, within the experimental error, with the difference ΔE_c–ΔE_{redox} = 140 mV between the positions of the conduction band and the redox levels in the two electrolytes. This result suggests that the change in R_{rec} is mostly due to these changes in the energetic levels. A change in slope is also found in the recombination resistance, which suggests that the recombination mechanism is also different. The small difference found between the shift in R_{rec} and the change in V_{oc} with the redox couples is also attributed to the change in slope of R_{rec}, since for lower slopes larger V_{oc} are expected.[9]

The significantly inferior FF is another important cause of the lower power conversion efficiency of the thiolate electrolyte. Through comparing the charge transfer resistances at the CE

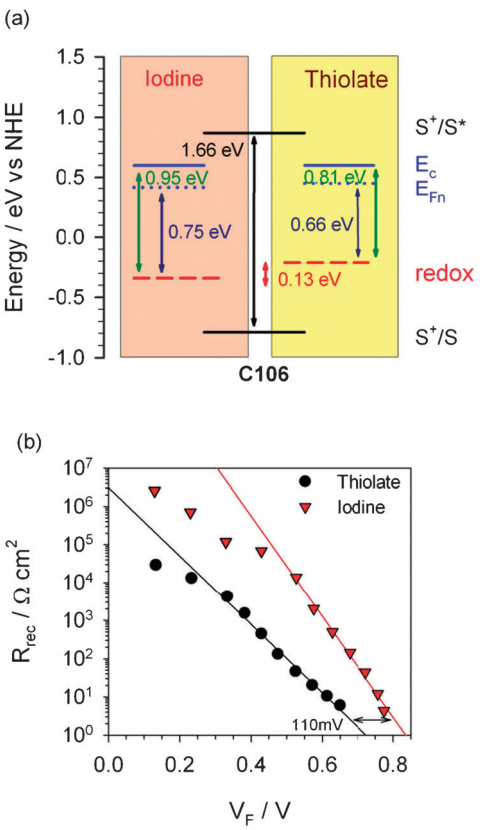

Fig. 4 (a) Energy levels in the DSCs sensitized with C106 in (left) iodine and (right) thiolate based electrolytes. (b) Recombination resistance for the DSCs with these two redox couples under 1 sun illumination.

(R_{CE}) in the two types of electrolyte, we found that the R_{CE} of thiolate is remarkably larger than that of the iodine cell, which is the main reason for the lower FF. Obviously, we may conclude here that the widely used Pt CE is not active enough for the reduction of T_2 in the thiolate electrolyte system.

Carbonaceous materials are usually considered as substitutes for Pt at counter electrodes in DSCs due to their high conductivity, large specific surface area and low cost, but the catalytic activities of carbonaceous materials for the reductive reaction on the CE are hardly comparable with Pt. We will utilize carbon black and several conductive polymer composites as active CEs for the thiolate electrolyte reduction, since conductive polymers have been proven to be highly active for electrocatalysis.[10] The pyrrole (PY), aniline (ANI) or 3,4-ethylenedioxythiophene (EDOT) was polymerized on a conductive carbon black (CCB) film screen printed on FTO glass to form a polymer–CCB composite CE for the thiolate cells.

The *j*–*V* characteristics of DSCs with different CEs are presented in Fig. 5 together with the cells with bare CCB and platinized CCB CEs used as references. The photovoltaic data are collected in Table 2. The discrepancies in both short circuit photocurrent densities and open circuit photovoltages are negligible for all the cells with these five CEs. The differences in the FFs, which determine the power conversion efficiency, are more important. The FF of bare CCB CE is only 0.31, indicating that CCB has poor catalytic activity for this thiolate electrolyte. After Pt is deposited on the CCB film, the FF rises by more than one-fold relative to the bare CCB, and 22% with relative to the Pt deposited on FTO (Table 1). The three types of polymer and the CCB composite CEs all exhibit enhanced FFs in contrast to the bare CCB CE. While for pyrrol and polyaniline these increases reach moderate values of the FF, the FF for the PEDOT–CCB composite CE achieves the high value of 0.70, higher than that of the Pt–CCB composite CE. Thus, this cell has a high power conversion efficiency of 7.6% with thiolate as redox couple.

To study the catalytic activity for the reduction of T_2 on these CEs, we performed electrical impedance spectroscopy (EIS) measurements on the cells based on the five CEs at the open circuit condition under the illumination of an LED. Fig. 6 shows the Nyquist plots of the thiolate electrolyte based DSCs with these five CEs. In a typical EIS analysis of a DSC, the charge transfer resistance at the counter electrode, R_{CE}, can be determined by the semicircle at the highest frequency regime.

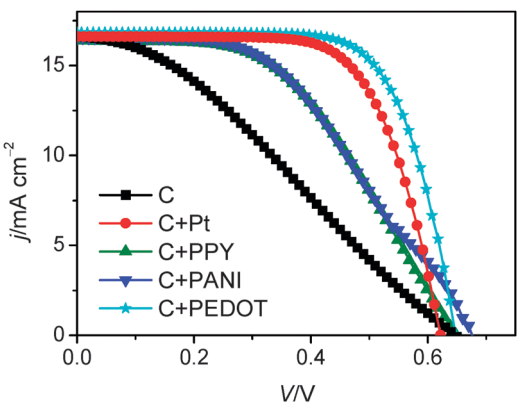

Fig. 5 *j*–*V* characteristics of DSCs with various CEs.

Table 2 Photovoltaic data of DSCs with various CEs under an irradiation of 100 mW cm^{-2} AM1.5G sunlight

CE	V_{oc}/mV	j_{sc}/mA cm^{-2}	FF	η (%)	R_{CE}/Ω
C	650 ± 4	16.6 ± 0.02	0.31 ± 0.001	3.4 ± 0.04	70
C + Pt	630 ± 4	16.6 ± 0.02	0.67 ± 0.002	7.0 ± 0.05	4
C + PPY	650 ± 5	16.4 ± 0.03	0.49 ± 0.002	5.2 ± 0.05	26
C + PANI	680 ± 4	16.5 ± 0.02	0.46 ± 0.003	5.2 ± 0.04	26
C + PEDOT	650 ± 5	16.8 ± 0.03	0.70 ± 0.003	7.6 ± 0.05	2

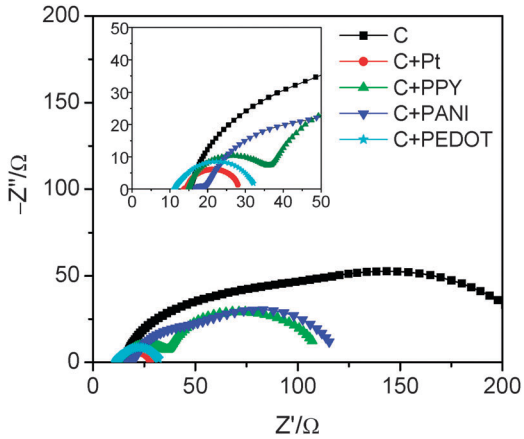

Fig. 6 Nyquist plots of the thiolate electrolyte based DSCs with various CEs at the open circuit condition under a LED illumination. The inset is an expansion of the high frequency regime.

R_{CE} represents the catalytic activity of the counter electrode. In Table 2 the direct relation between the FF and the R_{CE} can be clearly seen as the samples with a larger R_{CE} present a lower FF.

Conclusions

In summary, we have analyzed the intrinsic origins of the electrolyte influences on the photovoltaic parameters of dye-sensitized solar cells based on thiolate and iodine electrolytes, respectively, in conjunction with the high-absorptivity ruthenium dye C106. Transient absorption measurements show that the rate of dye regeneration by thiolate ions is slower than that by iodine ions, but both of them overwhelm the oxidized dye recombination with injected electrons, leading to the nearly 100% net charge generation yields. Furthermore, the comparable electron injection yields for the respective thiolate and iodine cell lead to similar IPCE maxima. The main origin of the difference in the V_{oc} has been attributed to the changes in the Fermi level of the thiolate electrolyte, which is 0.13 V more negative than that of the iodine congener. The change in the redox potentials, with a small contribution from the conduction band shift, produces an acceleration in the electron recombination process for T_2, pulling down the V_{oc} of the thiolate cell. The poor FF observed for thiolate originates in the large charge transfer resistance found at the platinized FTO. It has been proven that the charge transfer at the CE may be optimized by employing the highly active PEDOT–CCB composite as a CE. We combine a polymer–carbon black composite counter electrode with a high-absorptivity ruthenium dye C106 sensitized titania film, achieving an impressive efficiency on the DSCs with a non-corrosive organic thiolate electrolyte.

Experimental

Counter electrode preparation

The fluorine-doped tin oxide (FTO) glass substrates (TEC 15 Ω sq.$^{-1}$, Libbey-Owens-Ford Industries, 2.2 mm thick) were cleaned ultrasonically in deionized water, acetone and ethanol and finally dried by blowing them with dry air. The conductive carbon black (Super p) (CCB) paste was prepared by mixing CCB, polyvinylidene fluoride and *N*-methyl-2-pyrrolidone at a mass ratio of 16 : 9 : 180. A ~3.6 μm-thick CCB layer was first screen-printed onto a pre-cleaned FTO glass (TEC 15 Ω sq.$^{-1}$, Libbey-Owens-Ford Industries, 2.2 mm thick) and further baked at 120 °C for 5 min to produce a CCB positive electrode for the DSCs. The polymerization deposition was carried out by cyclic voltammetry technology using a three-electrode system. The working electrode was the FTO with CCB layer, the CE was a freshly polished Pt wire and the reference electrode was Ag–AgCl. The applied voltage range for PPY, PEDOT and PANI is −0.4 to 0.8, −0.4 to 1.2 and −0.6 to 1.0 V, respectively (scan times: three; scan rate: 10 mV s^{-1}). The electrolyte for PPY or PEDOT was composed of 0.1 M lithium bis(trifluoromethanesulfonyl)imide (LiTFSI) and 20 mM PY or EDOT in acetonitrile.[11] The aniline was polymerized in aqueous solution with 1 M HCl and 20 mM aniline.[12]

Cell fabrication and characterizations

A double-layer titania film was used as the negative electrode of the DSC. A 7 μm-thick transparent layer of 22 nm-sized TiO_2 particles was first screen-printed onto a pre-cleaned FTO conducting glass electrode (Nippon Sheet Glass, Solar, 4 mm thick) and further coated with a 6 μm-thick second layer of scattering titania particles (WERO-4, Dyesol). The detailed preparation procedures of the 22 nm-sized titania nanoparticles, pastes for screen-printing and nanostructured titania films were reported previously.[13] The film thickness was monitored with a bench-top Ambios XP-1 stylus profilometer. After sintering at 500 °C and cooling to 100 °C, the sintered titania electrodes (~0.28 cm^2) were stained by immersing them into a dye solution of C106 (10 mM C106 and 10 mM chenodeoxycholic acid in DMSO) for 5 min. The synthesis of C106 has been described in our previous paper.[14] The dye-coated titania electrode was then rinsed with DMSO and ethanol, dried by air flow, and was further assembled with a thermally platinized FTO or CCB–polymer composite printed FTO positive electrode by a 30 μm-thick Bynel (DuPont) hot-melt gasket and sealed up by heating. The internal space was perfused with a thiolate or iodine electrolyte with the aid of a vacuum-back-filling system. The thiolate electrolyte is composed of 0.4 M 5-mercapto-1-methyltetrazole ion (T^-), 0.2 M of the dimer of T^- (T_2) (Fig. S1†), 1 M 4-tert-pyridine (TBP) and 0.05 M lithium bis(trifluoromethanesulfonyl)imide (LiTFSI) in acetonitrile. The iodine electrolyte consists of 1.0 M 1,3-dimethylimidazolium iodide (DMII), 0.02 M iodine (I_2), 1.0 M TBP and 0.05 M LiI in acetonitrile.

Electrical impedance measurements

Electrical impedance experiments were carried out under an LED irradiation of 100 mW cm^{-2} on an IM6ex electrochemical workstation, with a frequency range from 50 mHz to 100 kHz and a potential modulation of 10 mV. The obtained impedance spectra were fitted with the Z-view software (v2.80, 2002, Scribner Associates Inc.) in terms of an appropriate equivalent circuit.

Voltammetric measurements

Square-wave voltammograms of ferrocene were measured on a CHI660C electrochemical workstation. A reference electrode was constructed by dipping a platinum wire into a DSC (thiolate or iodine) electrolyte-filling glass tube, the bottom end of which was sealed with a ceramic porous frit. A 5 μm-radius platinum ultramicroelectrode was used as the working electrode and a platinum wire as the CE.

Steady-state and transient absorption measurements

Electronic absorption spectra were recorded on a PerkinElmer Lamda 900 spectrometer. Transient absorption measurements were performed with a LP920 laser flash spectrometer pumped with a nanosecond wavelength tunable OPOLett-355II laser. The sample was kept at a 45° angle with respect to the excitation beam. The transient absorption spectrum was recorded with an Andor ICCD camera using a xenon arc lamp as the probe light. In the kinetic measurements, the probe light was first passed through a bandpass filter (center wavelength: 782 nm), detected by a fast photomultiplier tube and recorded with a TDS 3012C digital signal analyzer. The pulse fluence and excitation wavelength for the thiolate are 48.5 μJ cm^{-2} and 686 nm, for the iodine are 48.5 μJ cm^{-2} and 687 nm, and for the inert electrolyte are 48.2 μJ cm^{-2} and 690 nm, respectively.

Acknowledgements

The Chinese group thanks the National Science Foundation of China (No. 51103146), the National 863 Program (No. 2011AA050521) and the National 973 Program (No. 2011CBA00702) for financial support. We are grateful to Dyesol for supplying the WER4-O scattering paste and to DuPont Packaging and Industrial Polymers for supplying the Bynel film. The Spanish group acknowledges financial support from Ministerio de Cíencia e Innovación under Projects HOPE CSD2007-00007 and MAT 2010-19827 and Generalitat Valenciana under Project PROMETEO/2009/058.

Notes and references

1 B. O'Regan and M. Grätzel, *Nature*, 1991, **353**, 737.
2 G. Boschloo and A. Hagfeldt, *Acc. Chem. Res.*, 2009, **42**, 1819.
3 S. Yanagida, Y. Yu and K. Manseki, *Acc. Chem. Res.*, 2009, **42**, 1827.
4 (*a*) G. Oskam, B. V. Bergeron, G. J. Meyer and P. C. Searson, *J. Phys. Chem. B*, 2001, **105**, 6867; (*b*) H. Nusbaumer, J.-E. Moser, S. M. Zakeeruddin, M. K. Nazeeruddin and M. Grätzel, *J. Phys. Chem. B*, 2001, **105**, 10461; (*c*) S. A. Sapp, C. M. Elliott, C. Contado, S. Caramori and C. A. Bignozzi, *J. Am. Chem. Soc.*, 2002, **124**, 11215; (*d*) H. Nusbaumer, S. M. Zakeeruddin, J.-E. Moser and M. Grätzel, *Chem.–Eur. J.*, 2003, **9**, 3756; (*e*) P. Wang, S. M. Zakeeruddin, J.-E. Moser, R. Humphry-Baker and M. Grätzel, *J. Am. Chem. Soc.*, 2004, **126**, 7164; (*f*) P. J. Cameron, L. M. Peter, S. M. Zakeeruddin and M. Grätzel, *Coord. Chem. Rev.*, 2004, **248**, 1447; (*g*) Z.-S. Wang, K. Sayama and H. Sugihara, *J. Phys. Chem. B*, 2005, **109**, 22449;

(*h*) S. Hattori, Y. Wada, S. Yanagida and S. Fukuzumi, *J. Am. Chem. Soc*., 2005, **127**, 9648; (*i*) B. V. Bergeron, A. Marton, G. Oskam and G. J. Meyer, *J. Phys. Chem. B*, 2005, **109**, 937; (*j*) S. Cazzanti, S. Caramori, R. Argazzi, C. M. Elliott and C. A. Bignozzi, *J. Am. Chem. Soc*., 2006, **128**, 9996; (*k*) Z. Zhang, P. Chen, T. N. Murakami, S. M. Zakeeruddin and M. Grätzel, *Adv. Funct. Mater*., 2008, **18**, 341; (*l*) B. M. Klahr and T. W. Hamann, *J. Phys. Chem. C*, 2009, **113**, 14040; (*m*) C. Teng, X. Yang, C. Yuan, C. Li, R. Chen, H. Tian, S. Li, A. Hagfeldt and L. Sun, *Org. Lett*., 2009, **11**, 5542; (*n*) T. C. Li, A. M. Spokoyny, C. She, O. K. Farha, C. A. Mirkin, T. J. Marks and J. T. Hupp, *J. Am. Chem. Soc*., 2010, **132**, 4580; (*o*) H. Wang, P. G. Nicholson, L. Peter, S. M. Zakeeruddin and M. Grätzel, *J. Phys. Chem. C*, 2010, **114**, 14300; (*p*) H. Tian, X. Jiang, Z. Yu, L. Kloo, A. Hagfeldt and L. Sun, *Angew. Chem., Int. Ed*., 2010, **49**, 7328; (*q*) M. Wang, N. Chamberland, L. Breau, J.-E. Moser, R. Humphry-Baker, B. Marsan, S. M. Zakeeruddin and M. Grätzel, *Nat. Chem*., 2010, **2**, 385; (*r*) S. Caramori, J. Husson, M. Beley, C. A. Bignozzi, R. Argazzi and P. C. Gros, *Chem.–Eur. J*., 2010, **16**, 2611; (*s*) S. M. Feldt, E. A. Gibson, E. Gabrielsson, L. Sun, G. Boschloo and A. Hagfeldt, *J. Am. Chem. Soc*., 2010, **132**, 16714; (*t*) D. Li, H. Li, Y. Luo, K. Li, Q. Meng, M. Armand and L. Chen, *Adv. Funct. Mater*., 2010, **20**, 3358; (*u*) A. Yella, H.-W. Lee, H. N. Tsao, C. Yi, A. K. Chandiran, M. K. Nazeeruddin, E. W.-G. Diau, C. Y. Yeh, S. M. Zakeeruddin and M. Grätzel, *Science*, 2011, **334**, 629; (*v*) T. W. Hamann and J. W. Ondersma, *Energy Environ. Sci*., 2011, **4**, 370.

5 Selected examples include: (*a*) A. Kay and M. Gratzel, *Sol. Energy Mater. Sol. Cells*, 1996, **44**, 99; (*b*) K. Imoto, K. Takahashi, T. Yamaguchi, T. Komura, J. Nakamura and K. Murata, *Sol. Energy Mater. Sol. Cells*, 2003, **79**, 459; (*c*) K. Suzuki, M. Yamaguchi, M. Kumagai and S. Yanagida, *Chem. Lett*., 2003, **32**, 28; (*d*) S. Jang, R. Vittal and K. Kim, *Langmuir*, 2004, **20**, 9870; (*e*) T. N. Murakami, S. Ito, Q. Wang, M. K. Nazeeruddin, T. Bessho, I. Cesar, P. Liska, R. Humphry-Baker, P. Comte, P. Pechy and M. Grätzel, *J. Electrochem. Soc*., 2006, **153**, A2255; (*f*) Z. Huang, X. Liu, K. Li, D. Li, Y. Luo, H. Li, W. Song, L. Chen and Q. Meng, *Electrochem. Commun*., 2007, **9**, 596; (*g*) T. N. Murakmi and M. Grätzel, *Inorg. Chim. Acta*, 2008, **361**, 572; (*h*) W. Hong, Y. Xu, G. Lu, C. Li and G. Shi, *Electrochem. Commun*., 2008, **10**, 1555; (*i*) W. J. Lee, E. Ramasamy, D. Y. Lee and J. S. Song, *ACS Appl. Mater. Interfaces*, 2009, **1**, 1145; (*j*) M. X. Wu, X. Lin, T. H. Wang, J. S. Qiu and T. L. Ma, *Energy Environ. Sci*., 2011, **4**, 2308; (*k*) H. Wang, G. Liu, X. Li, P. Xiang, Z. Ku, Y. Rong, M. Xu, L. Liu, M. Hu, Y. Yang and H. Han, *Energy Environ. Sci*., 2011, **4**, 2025.

6 (*a*) S. Ardo and G. J. Meyer, *Chem. Soc. Rev*., 2009, **38**, 115; (*b*) S. A. Haque, Y. Tachibana, R. L. Willis, J. E. Moser, M. Grätzel, D. R. Klug and J. R. Durrant, *J. Phys. Chem. B*, 2000, **104**, 538; (*c*) S. Pelet, J.-E. Moser and M. Grätzel, *J. Phys. Chem. B*, 2000, **104**, 1791.

7 (*a*) S. E. Koops, B. C. O'Regan, P. R. F. Barnes and J. R. Durrant, *J. Am. Chem. Soc*., 2009, **131**, 4808; (*b*) C. A. Kelly, F. Farzad, D. W. Thompson, J. M. Stipkala and G. J. Meyer, *Langmuir*, 1999, **15**, 7047.

8 E. M. Barea, J. Ortiz, F. J. Payá, F. Fernández-Lázaro, F. Fabregat-Santiago, A. Sastre-Santos and J. Bisquert, *Energy Environ. Sci*., 2010, **3**, 1985.

9 F. Fabregat-Santiago, J. Bisquert, E. Palomares, L. Otero, D. Kuang, S. M. Zakeeruddin and M. Grätzel, *J. Phys. Chem. C*, 2007, **111**, 6550.

10 B. Winther-Jensen, O. Winther-Jensen, M. Forsyth and D. R. MacFarlane, *Science*, 2008, **321**, 671.

11 (*a*) Y. Saito, W. Kubo, T. Kitamura, Y. Wada and S. Yanagida, *J. Photochem. Photobiol., A*, 2004, **164**, 153; (*b*) S. Ahmad, M. Deepa and S. Singh, *Langmuir*, 2007, **23**, 11430; (*c*) J. Wu, Q. Li, L. Fan, Z. Lan, P. Li, J. Lin and S. Hao, *J. Power Sources*, 2008, **181**, 172.

12 (*a*) A. G. MacDiarmid, *Angew. Chem., Int. Ed*., 2001, **40**, 2581; (*b*) G. Wu, K. L. More, C. M. Johnston and P. Zelenay, *Science*, 2011, **332**, 443.

13 P. Wang, S. M. Zakeeruddin, P. Comte, R. Charvet, R. Humphry-Baker and M. Grätzel, *J. Phys. Chem. B*, 2003, **107**, 14336.

14 Y. Cao, Y. Bai, Q. Yu, Y. Cheng, S. Liu, D. Shi, F. Gao and P. Wang, *J. Phys. Chem. C*, 2009, **113**, 6290.

